Published in, Proc. of the International Symposium on Non-Steady Fluid Dynamics, ASME FED Vol. 92, Toronto, Canada, June 4-7, 1990, pp. 253-258.

CONVECTIVE RESPONSE OF A WALL-MOUNTED HOT-FILM SENSOR IN A SHOCK TUBE

A. Sidney Roberts, Jr.,[1] Kelly R. Ortgies[2] and Ehud Gartenberg[3]
Department of Mechanical Engineering and Mechanics
Old Dominion University, Norfolk, Virginia USA

and

Debra L. Carraway[4]
NASA Langley Research Center
Hampton, Virginia USA

ABSTRACT

Recent efforts with arrayed hot-film sensors, maintained at constant temperature and mounted flush with an airfoil surface, are directed toward detecting the various modes of change in the boundary layer flow regimes. Shock tube experiments have been performed in order to determine the response of a single hot-film element of a sensor array to transiently induced flow behind weak normal shock waves. The experiments attempt to isolate the response due only to the change in convective heat transfer at the hot-film surface mounted on the wall of the shock tube. The experiments are described, the results being correlated with transient boundary layer theory and compared with an independent set of experimental results. One of the findings indicates that the change in the air properties (temperature and pressure) precedes the air mass transport, causing an ambiguity in the sensor response to the development of the velocity boundary layer. Also, a transient, local heat transfer coefficient is formulated to be used as a forcing function in an hot-film instrument model and simulation which remains under investigation.

INTRODUCTION

Shock tube experiments have been performed to determine the response of one element of an arrayed hot-film sensor, mounted flush on the side-wall of the tube, to the flow induced by weak normal shock waves. The experiments attempt to isolate the response of the anemometer due only to the change in convective heat transfer at the hot-film surface. The work is the result of collaborative efforts with NASA Langley Research Center, Hampton, Virginia, USA, where a primary goal has been the refinement of a hot-film sensor able to detect the development of perturbations in the laminar boundary layer.

[1]Professor
[2]Graduate Research Assistant
[3]Research Assistant Professor
[4]Aerospace Engineer

The continuing effort to develop this type of constant temperature hot film sensor is specifically aimed at the detection of the various types of identified modes of boundary layer instability, for example Tollmein-Schlichting waves, Goertler and crossflow vortices (Wusk, et al., 1988). The particular effort with the arrayed sensors, concentrating on both the sensor design, fabrication and signal processing, is intended to provide an experimental tool capable of detecting spanwise patterns of vortical striations with a spatial resolution better than two and one-half millimeters (0.1 inch) per wavelength and a frequency response up to 1×10^5 Hz (Wusk, et. al., 1988 and Ortgies, 1989). The ultimate goal is to qualify these sensors for flight tests in order to gather data concerning laminar boundary layer instabilities under operational conditions. Among the performance parameters characterizing the sensor, the limit of its time response is the most difficult one to predict. A local variation in the convective heat transfer characteristic of the airflow will influence both the sensor and the surrounding areas of the substrate. An analytic effort to understand the influence of the substrate involvement on the arrayed sensor response was carried out by McRee and Judge (1987), who set out to model the complete instrument behavior starting with both convection and conduction heat dissipation modes and ending with an electronic circuit response. Initially, this model used a sinusoidally varying convective heat transfer coefficient as a forcing function in order to predict the anemometer (sensor, substrate and circuit) response to a cyclical change in the flow conditions. However, to make a prediction of the sensor's response due to vortical flow conditions, it was necessary to input a time dependent convective heat transfer coefficient characteristic of vortical flows, but such a function was not available.

In order to produce some characteristic values of the convective heat transfer coefficient resulting from actual transient flow conditions, recourse was made to shock tube testing. This decision was supported by the fact that the flowfield induced by the moving compression wave approximates a step velocity change with respect to time. Furthermore, the flow behind the shock wave both in the free

stream and in the boundary layer, is amenable to analytic treatment (Anderson, Jr., 1982, and Mirels, 1955 and 1956 respectively).

The following sections describe in turn the experimental methods, analysis of the results, and the conclusions drawn. The experiments were carried out in a 15.2 cm (6 inch) diameter shock tube at the Instrument Research Division of NASA Langley Research Center. The hot-film sensors were mounted on a plug fitted flush with the inside surface of the cylindrical test section wall as described below. The flow velocity was deduced from piezoelectric pressure transducer data, the change in convective heat transfer from the hot-film anemometer, and the results were compared with those from Mirels' transient boundary layer theory (Mirels, 1956) and the experimental shock tube data of Davis and Bernstein (1969).

EXPERIMENTAL METHOD

An array of four nickel film sensors (0.51x0.76 mm each) was mounted on an insulating foam plug inserted through the cylindrical wall of the shock tube. Only one sensor was active, and maintained at constant temperature during the experiments. The built-up sensor presented a roughness element of 0.1 mm or less at the inside wall surface in the test section. A piezoelectric pressure transducer was mounted opposite the hot-film sensor plug. Another piezoelectric pressure transducer was mounted 61.0 cm upstream from the hot-film sensor, allowing an independent time-of-flight measurement of shock motion. Figure 1 is a schematic diagram showing the shock tube layout, position of sensors, and the instrumentation assembly. It may be noted that the 7.62 cm (3 inch) diameter driver section is followed immediately by a diverging section with an area ratio of 4. At low supersonic shock speeds, where the induced free stream flow is subsonic, this diverging section acts as a subsonic flow diffuser.

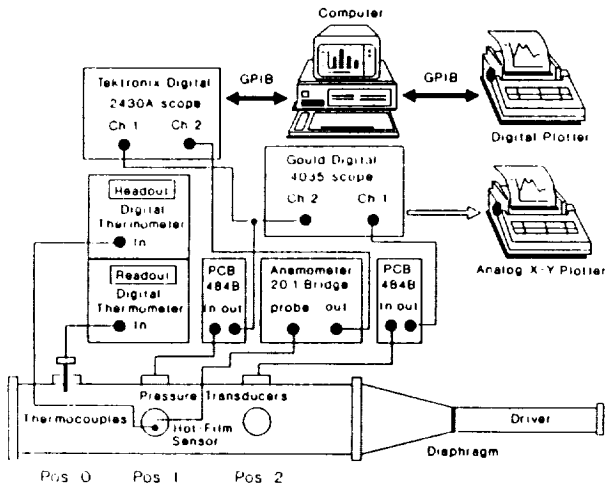

Figure 1. Equipment Schematic for Shock Tubes Tests

The sensor was set to a nominal temperature of 380 K (an overheat of about 85 K above ambient) and allowed to reach a thermal steady state with the plug and the ambient air prior to breaking a Mylar diaphragm in the driver (air) section. The sequence of tests was performed at three sensor temperatures, corresponding to overheat ratios (ratio of the heated sensor resistance to the cold sensor resistance) of 1.3, 1.4 and 1.5. The effect of increasing the sensor temperature was to increase the anemometer sensitivity to flow fluctuations and increase the frequency response of the anemometer. The substrate temperature, measured at the thermocouple location on the plug surface, maintained approximately the same average temperature (22.8 ± 0.6 °C) throughout the series of tests for all three overheat ratios.

Before each test, the end plate of the shock tube was removed and the debris remaining inside the tube due to the diaphragm rupture was blown out, in order to minimize the amount of flow disturbance present during a test. The Mylar diaphragm was cut from a sheet with thickness corresponding to an estimated driver rupture pressure, and the diaphragm was inserted into its holder and placed in position in the shock tube (see Fig. 1). A computer program was implemented to initialize the Tektronix Oscilloscope parameters and store the anemometer digitized voltage signals and position 1 pressure transducer response data. After these procedures were completed, the driver section was pressurized until the diaphragm ruptured. At the time of the diaphragm rupture, the maximum driver pressure attained was recorded from a Wallace and Tierman pressure gauge. Subsequently, the oscilloscope captured the transient anemometer and "position 1" pressure transducer response data as the shock passed the hot-film sensor. Tests were conducted at driver gauge pressures of approximately: (1) 179 kPa (26 psig), (2) 338 kPa (49 psig), (3) 386 kPa (56 psig), to (4) 545 kPa (79 psig). In most tests of interest, the ratio of the shocked gas to undisturbed air pressure, P_2/P_1, was 1.3. At each of the driver pressures, tests were repeated for which the time base of the oscilloscope was changed from 500 μs/div to 20 μs/div. The maximum experiment time, determined by the arrival of the reflected shock, was about 3 milliseconds.

The active hot-film sensor in the constant temperature anemometer circuit was found to have a frequency response (weakly variable with overheat ratio) of about 100 kHz, using a 30 kHz square wave test. Data acquired by the oscilloscope for each test, the passage of the shock front across the sensor station, was down-loaded to a floppy disk. Knowing the anemometer circuit and overheat parameters, the voltage versus time values were transformed to convected power versus time values (or local Reynolds numbers) as an indication of the time dependent convection heat transfer coefficient. The initial conduction and radiation heat transfer rates prior to shock passage remained essentially unchanged as the transient boundary layer flow developed over the sensor, because of the large thermal inertia of the sensor substrate and the constancy of the sensor temperature.

RESULTS

Figure 2 displays the anemometer response versus time along with the corresponding pressure transducer response. Incident and reflected shock transients are clearly distinguished, and on an expanded time base both transducers demonstrate a rise time corresponding to $1x10^5$Hz (see Figure 5). The shocked gas pressure (P_2), taken from Figure 2 (a), in ratio with the ambient pressure (P_1) are used to determine the shock speed from normal shock tables for air; the deduced speed agrees to within one percent with the values from the independent time-of-flight measurements of the shock front between the pressure transducers. Test or experiment numbers are designated by the prefix, "Exp." in the figures. As noted previously,

the anemometer voltage signals (Figure 2 (b)) are transformed to convected power-versus-time results. The convected power results appear the same as those shown in Figure 2(b) after the dc-level reference power, prior to shock arrival, is subtracted. Two interesting features of the anemometer response received further study: the leading dip in convected power (reduced heat transfer from the sensor), and the initial decrease in the power convected away from the sensor surface during the first millisecond after the incident shock passes across the sensor. From shock speed measurements, the transit time of the shock across the sensor is about 2.0 microseconds. It is hypothesized that as the incident wave passes across the sensor, the step change in the shocked gas temperature precedes the development of the velocity boundary layer that begins to grow more slowly due to a mass transport lag. These effects are discussed in detail below.

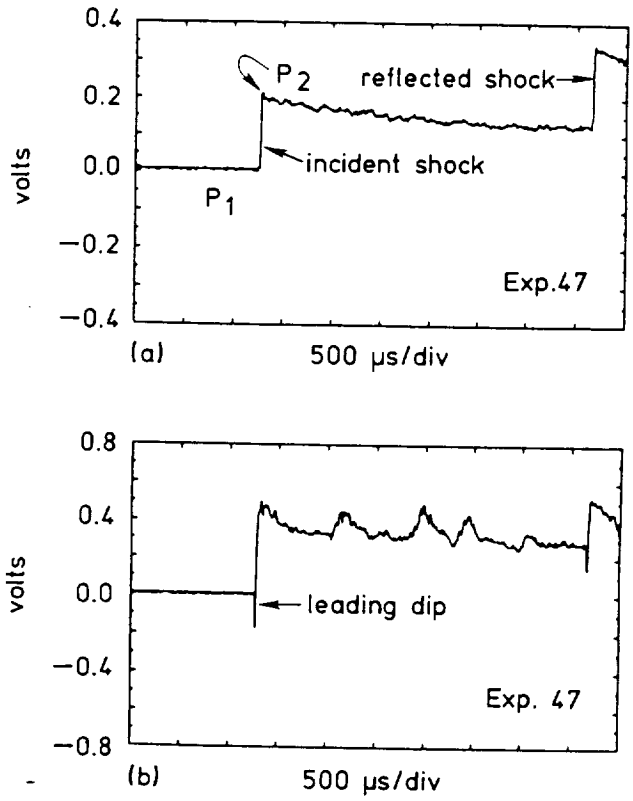

Figure 2. Signal Response at a Driver Pressure of 183 kPa (26.5 psig) for the (a) Pressure Transducer, and (b) Anemometer

Most of the data presented here are results from experiments performed at a low shock pressure ratio, P_2/P_1 = 1.28, which is the basis for the anemometer response in Figure 2. Figure 3, however, shows how the anemometer response dramatically changes when a stronger shock (P_2/P_1 = 1.60) is induced. While not well understood, the case in Figure 3(b) suggests a fully developed turbulent flow, quite different from the lower frequency, intermittent response found at the lower shock speed in Figure 3(a). A recent paper (Johnson and Carraway, 1989), describing experiments with hot films on flat plates in supersonic flow, attributes the intermittency to boundary layer transitional effects, and the lower amplitude, higher frequency signal to fully developed turbulent flow. The thrust herein is to treat the evidence for boundary layer development during the first millisecond of the low pressure ratio runs, and to correlate the data with boundary layer theory due to Mirels (1956).

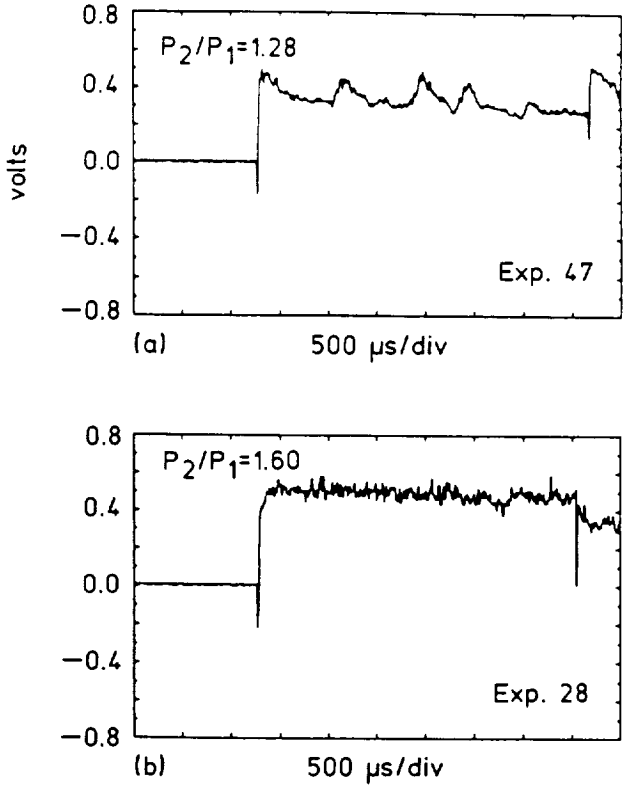

Figure 3. Comparison of Anemometer Response at Driver Pressures of (a) 183 kPa (26.5 psig), and (b) 543 kPa (78.8 psig).

Table 1 summarizes pertinent experimental findings in terms of directly measured quantities and deduced, calculated quantities.

The value P_4 is the driver gas pressure; P_1 is the undisturbed gas pressure; T_b is ambient temperature; T_{sub} is the substrate temperature (essentially unchanged during experiments); T_w is the sensor surface temperature, U_w is the shock speed; P_2/P_1 is the shocked gas pressure ratio; $\overline{U}_e$ is the induced freestream speed of flow behind the shock; T_e is the shocked gas temperature; T_r is the recovery temperature; and, $h^*(t)^{0.2}$ is the calculated theoretical convective heat transfer coefficient (Ortgies, 1989) for a turbulent boundary layer. The interpretation of a transient, turbulent boundary layer development during the first millisecond of the experiment shown in Figure 3(a) is based on Mirels' theory (1955 and 1956), where a steady boundary layer problem may be solved in the frame of reference of the moving shock. When the convected power versus time data, which according to the theory should be a power law relationship, is graphed logarithmically a straight line fit is found. In nondimensional Stanton number — Reynolds number form slope parameters of –0.17, –0.25, –0.18 are found respectively for the three cases reported in Table 1, and the corresponding correlation coefficients (r^2) are 0.827, 0.879 and 0.889. A comparison with the Mirels' theory, where the slope should be, -0.20, for turbulent

Table 1. Measured and Calculated Experiment Parameters†

Measured									Calculated			
Exp. No	P_4 (kPa) gauge	P_1 (kPa) absolute	T_b (K)	T_{sub} (K)	T_w (K)	U_w (m/s)	P_2/P_1	Over Heat Ratio	$\overline{U}_e$ (m/s)	T_e (K)	T_r (K)	$h^* \cdot t^{0.2}$ (W $ms^{0.2}/m^2K$)
22	186	103	295	296	380	385	1.29	1.3	65	318	320	220
39	185	103	295	296	400	383	1.29	1.4	62	317	319	216
47	183	103	295	296	421	383	1.28	1.5	62	317	318	214

†Expected error in the parameters in implied by the number of significant figures reported.

boundary layer development, is shown in Figure 4. It is seen from Figure 4 that the experimental Stanton number is higher than theory predicts for the same Reynolds number. This trend is repeated for the other two test cases, which are not shown. Plotted with the theoretical and experimental heat transfer correlations in Figure 4 is the Stanton number correlation which fits the Davis and Bernstein (1969) experimental data set. There was no evidence of a laminar-to-turbulent transition, seen in the current work, even though the results fall well below the critical Reynolds number for flat plate boundary layer flow.

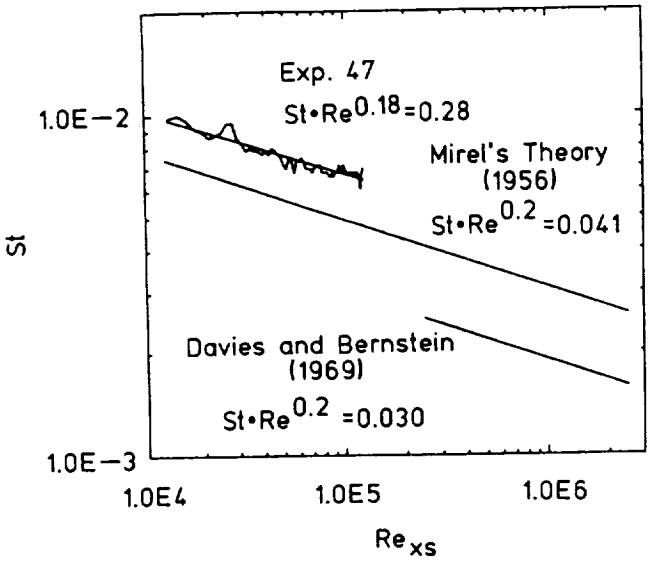

Figure 4. Comparison of Experimental and Theoretical Heat Transfer Results. Re_{xs} is a Reynolds Number Measured with Respect to the Shock Position

As noted earlier, an interesting development occurs as the shock passes the hot-film sensor. A very pronounced dip occurs in the anemometer signal a few microseconds after the shock front reaches the sensor. Figure 5 shows the experimental data record on a 20μs/div time-base for an expanded view. Excited by the transient, the hot-film sensor response drops negatively until it reaches a minimum. It then increases sharply to realize a maximum within the 25μs time frame. During the course of the experiments, the magnitude of the voltage drop was seen to increase with increasing driver pressure P_4, as illustrated in Figure 5. As seen in Figure 5(a), when P2/P1 = 1.28, the drop was approximately 0.27 V. In Figure 5(b), where P2/P1 = 1.61, the drop was 0.55V. The data obtained was repeatable and the trend was without exception. No other experimental works have been found which discuss this leading negative-going pulse in the hot-film sensor response.

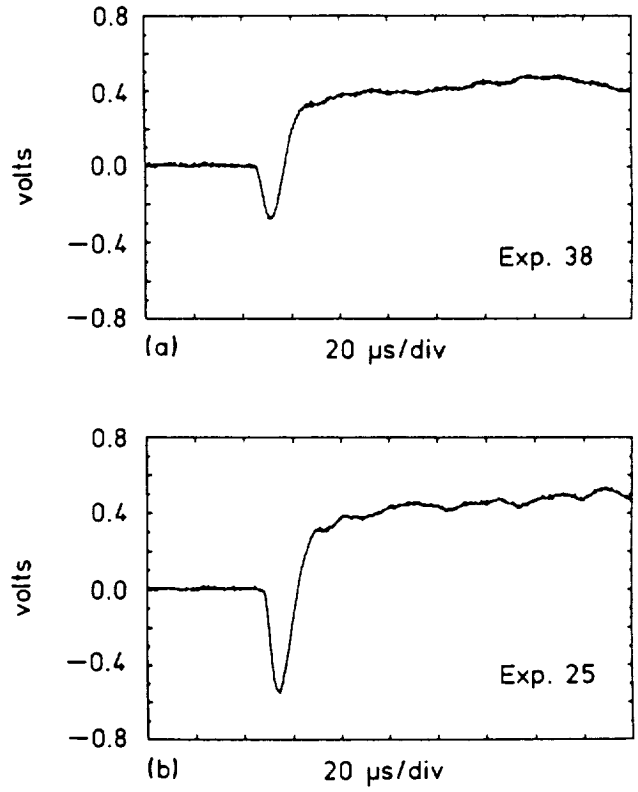

Figure 5. Anemometer Response Showing Wave Transit Effect, P_4 = (a) 181 kPa, and (b) 531 kPa Gauge Pressure

A hypothesis is generated in order to explain the phenomenon of this drop in voltage, which corresponds to a decrease in the convective heat transfer from the hot-film sensor. It is known that as the shock passes across the hot-film sensor, the temperature of the

free stream gas behind the wave rises abruptly. It is further hypothesized that the step change in free stream temperature across the shock wave precedes the development of the velocity boundary layer because of a mass transport lag. Consequently, natural convective conditions may prevail just prior to the build-up of the shocked gas velocity boundary layer, but sensor/substrate to free stream gas temperature differences are now less. Thus, a smaller temperature difference along with natural convective heat transfer produces a sudden decrease in the heat flux from the sensor. Note that the substrate adjacent to the sensor maintains a temperature, T_{sub}, some 22°C below the shocked gas temperature, T_e (see Table 1). The current supplied to the hot-film sensor to maintain its constant operating temperature is decreased, which produces the initial drop seen in the experimental results for the first few microseconds of the test. At the start of the velocity boundary-layer growth the heat flux from the sensor is a maximum since the forced convective heat transfer coefficient becomes large. As the velocity boundary layer grows, the heat flux from the sensor decreases and the anemometer supplies less current to maintain the constant operating temperature of the hot-film sensor, which is the effect detected during the first millisecond and seen more clearly in Figure 3(a).

The estimate of a natural convective heat transfer coefficient is made by assuming a characteristic length equal to the area of the sensor divided by the length of the sensor (0.762 mm). It is also assumed that this characteristic length can be associated with a small wire (horizontal cylinder). With these assumptions, Morgan (1975) defines a natural convective correlation for various ranges of Grashof numbers. After calculating the Grashof number (approximately 0.12) and applying the correlation given by Morgan (1975), an estimate of the natural convective heat transfer coefficient is made yielding a value of $8.0 \times 10^1 W/m^2 \cdot K \pm 25$ percent due to the uncertainty in the correlation.

The transient convective heat transfer coefficient is divided into three parts. The first is an estimate of the amount of natural convection occurring before the start of the test from the initial power being supplied to the sensor to maintain its operating temperature. Second, a heat transfer coefficient is needed from time t=0 to approximately t=25 μs which is based on the prior hypothesis. Finally, the transient response derived from Mirels (1956) for turbulent boundary layer development is used for times greater than measured shock transit times.

During the time that the output voltage drops dramatically and rises again ($0<t<25\mu s$), the heat transfer coefficient is assumed to be a constant. The calculated time for the shock to pass across the sensor ranges from 1.8 to 2.0 μs at the tested driver pressures, based on time-of-flight measurements. The measured time half-way across the negative anemometer pulse is on the order of 5 to 12 μs. A discrepancy exists between the calculated shock transit time across the sensor and the anemometer measured transit time. This discrepancy may be attributed in part to the lag associated with the mass transport of the gas behind the shock, but is more probably related to the response time of the anemometer. The inverse transit time of the shock moving across the sensor is larger by a factor of 5 than the frequency response of the anemometer (~100 kHz). Consequently, the anemometer may not be responding fast enough to capture the full effect of the shock transit.

The natural convective value of heat transfer coefficient is assumed valid during the shock transit time. The transient portion of the convective heat transfer coefficient is of the form shown in Table 1 for a turbulent boundary layer. By combining the three portions, a complete heat transfer coefficient is estimated for a given set of test conditions. Figure 6 shows a convective heat transfer coefficient curve for Exp. 47. Thus, a computer model can simulate the shock tube test cases using the combined heat transfer coefficient as a forcing function.

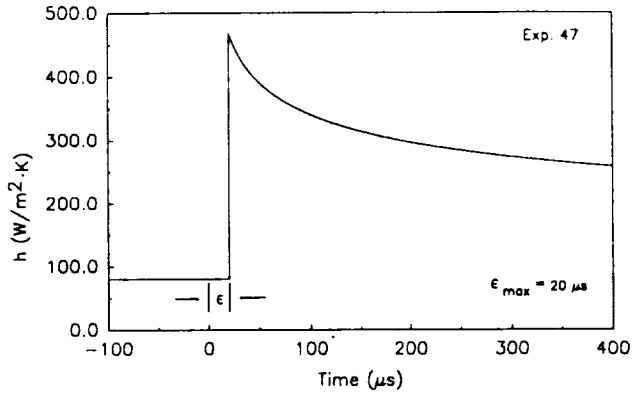

Figure 6. Transient Convective Heat Transfer Coefficient

CONCLUSIONS

The transient response of the hot-film anemometer has been analyzed with a combination of results. First, repeatable data is easily obtained over the range of driver pressures used. The experimental comparison of the data with transient, turbulent compressible boundary layer theory seems to be valid within the first millisecond of experiment time at driver pressures of approximately 179 kPa (26.0 psig). Even at these driver pressures with statistically valid curve fits, the theoretical Stanton number for turbulent flow is less than the Stanton number obtained from the experimental data. The slopes are similar (see Figure 5), but the coefficients have different values, and the current results find a turbulent boundary layer at Reynolds number below $1x10^5$. After the first millisecond the anemometer response becomes intermittent at the lower pressure ratios. This may be due to flow disturbances occurring inside the shock tube due to the diffuser, microcavities from the ports in the walls, or unsteady turbulent free stream flow.

The comparisons with other experimental work (Davies and Bernstein, 1969) indicate qualitative agreement. The analysis of the anemometer response at the higher driver pressures must be left to future testing under more strictly controlled conditions. A surprising result of this work is the occurrence of reduced convected heat transfer as the shock wave passes over the sensor. This effect has not been clearly demonstrated in the other experimental works examined by the authors. While an hypothesis is offered, further investigation is needed to fully understand this phenomenon.

The computer simulation of the anemometer response (McRee and Judge, 1987) is to be investigated in an extension of this project with hope that agreement between these experimental results and

predicted anemometer response will tend to validate the hot-film anemometer model.

ACKNOWLEDGEMENT

The study reported here was partially supported by NASA Langley Research Center grant NAG-1–735, managed by the Old Dominion University Research Foundation.

REFERENCES

Anderson, Jr., John D., 1982, Modern Compressible Flow, McGraw-Hill Book Co., New York, N.Y, Chap. 7.

Davies, W. R. and Bernstein, L., 1969, "Heat Transfer and Transition to Turbulence in the Shock-Induced Boundary Layer on a Semi-Infinite Flat Plate," J. Fluid Mechanics, Vol. 36, pp. 87–112.

Johnson, C. B. and Carraway, D. L., 1989, "A Transition Detection Study at Mach 1.5, 2.0, and 2.5 Using a Micro-Thin Hot-Film System", Proc. of the International Congress on Instrumentation in Aerospace Simulation Facilities, ICIASF '89, Goettingen, West Germany, pp. 82–94.

McRee, G. J. and Judge, D. M., 1987, "Model of Hot-Film Sensor with Substrate," Proc. of the International Congress on Instrumentation in Aerospace Simulation Facilities, ICIASF '87, Williamsburg, VA, pp. 350–355.

Mirels, H., 1955, "Laminar Boundary Layer Behind Shock Advancing into Stationary Fluid," NACA TN 3401, Washington, D.C..

Mirels, H., 1956, "Boundary Layer Behind Shock or Thin Expansion Wave Moving into Stationary Fluid," NACA TN 3712, Washington, D.C.

Morgan, T., 1975, "The Overall Convective Heat Transfer from Smooth Circular Cylinders," Advances in Heat Transfer, Vol. 11, Academic Press, New York.

Ortgies, K., 1989, "Transient Hot-Film Sensor Response in a Shock Tube," Masters thesis, Department of Mechanical Engineering and Mechanics, Old Dominion University, Norfolk, VA; also, NASA CR 181838.

Wusk, M. S., Carraway, D. L. and Holmes, B. J., 1988, "An Arrayed Hot-Film Sensor for Detection of Laminar Boundary-Layer Flow Disturbance Spatial Characteristics," AIAA Paper 88–4677–CP, AIAA/NASA/AFWAL Sensors and Measurement Technologies Conference, Atlanta, Georgia.

INFRARED SURFACE IMAGING AS A FLOWFIELD DIAGNOSTIC TOOL

by Ehud GARTENBERG, A. Sidney ROBERTS, Jr., and Gregory V. SELBY

Department of Mechanical Engineering and Mechanics
Old Dominion University
Norfolk, Virginia 23508 USA

Abstract

An infrared imaging system supported by a dedicated image processing system was evaluated as a diagnostic tool for aerodynamic research. The results reported herein characterize the system's capability in performing a variety of experimental investigations such as: temperature transients, air velocity distrubutions, capture of vortices, boundary layer flows and separated flows over a flat plate with a two-dimensional rearward-facing step.

1. INTRODUCTION

Infrared imaging systems are proving to be convenient experimental tools for surface temperature mapping. Their main advantages over the classical methods may be summarized as follows:

1) They are non-intrusive, thus permitting measurements without interfering with the phenomenon under investigation and also without the need to expose the sensor itself to potentially hostile environments.

2) They map continuously the whole region of interest (rather than discrete points), thus producing "frozen" pictures of the entire field, a feature of great importance when studying unsteady phenomena.

3) They have the output displayed on video screen, permitting real-time evaluation of the results, and allowing the investigator the flexibility of corrective actions while running the experiments.

The use of these systems has been extended to heat transfer research, e.g., from buildings to their surroundings [1]. There, the actual conditions were simulated by scale models in a stratification wind tunnel. Thereafter, the experimental data gathered as temperature contours were used to calculate local heat transfer coefficients. a logical follow-up is to apply this method to aerodynamic research by taking advantage of the inherent heat exchange phenomena between an aerodynamic surface and the surrounding fluid flow.

Basically speaking, there are two radically different ways of heating an aerodynamic surface and obtaining temperature distributions due to the energy interaction with the free stream. One method is through passive heating due to recovery of the freestream temperature in the stagnation areas and the boundary layer [2]. The other is by uniform active heating (e.g. by electrically heated elements) and variable local cooling due to the flowfield interaction with the surface.

For quantitative assessment, the raw IR data is digitally processed by dedicated software for image enhancement, allowing the capture of small local differences in temperature, that are barely detectable by the human eye in the original image [3].

The work reported herein was aimed at exploring the feasibility of using IR imagery in aerodynamic research, using actively-heated surfaces as targets, an AGA system for detection and imagery and image processing software for data extraction.

2. THE IR IMAGING AND PROCESSING SYSTEM

The nucleus of the IR imaging system is an AGA Thermovision 782 camera equipped with 20°x20° lens coated for optimal response in the short wave (5 μm) infrared spectrum. At 0.5-m distance, the field of view is 0.15 x 0.15-m. Throughout the reported experiments, the aperture was kept at f/1.8. The optical scanning system is syncronized such that four fields of 100 horizontal lines each, produce one interlaced frame. The scanning rate is 25 fields per second. The scanned field is reproduced on a specially-designed black-and-white video display unit, which facilitates direct or relative thermal level measurements. The angular resolution of the system in the above configuration is 0.003 radians.

Proceeding of the 12th International Congress on Instrumentation in Aerospace Simulation Facilities (Sponsored by IEEE)
The College of William and Mary
Williamsburg, Virginia
June 22-25, 1987

The digital image processing is performed on a dedicated BMC IF800, model 20 personal computer with 64K bytes main memory plus an extra 128K bytes RAM PCB and two 5 1/4" disk drives. The color CRT display has graphics capability.

A DISCO 2.0 software package is used for the image processing and completely occupies a floppy disk in a read-only storage mode. Up to 36 individual images can be stored on the second floppy disk in a read-and-write access storage mode. The automatic aquisition capability of the system permits continuous recording of up to 16 images at an approximate rate of 1.5 Hz or lower. Although both the field and frame aquisition modes are available, only the field mode was used. A key feature of this program is the gradual assignment of eight tones of artificial colors (from black through blue, green, red, etc., to white), for corresponding grey shades in the original image. Such a display produces a color shade for each temperature band scanned by the camera. The user has the choice of getting temperature measurements at a certain point or along specified rows or columns, for given values of the input parameters (emittance, transmittance, ambient temperature, etc.). Also, the user can concentrate on a given range of temperatures, depending on the area of interest. The program is quite versatile and offers an abundance of processing and filtering choices; however, only the essentials have been reported herein.

3. FEASIBILITY STUDIES

The IR imaging system can be used in conjunction with actively-heated aerodynamic surfaces in two ways. One way is to suspend a thin heated wire across a flowstream and to monitor the temperature variations along it. Assuming that the heat conduction along the wire is negligible compared to the forced convection, this method is particularly effective in capturing wakes and vortices. The other approach is to bond heated wires or strips on aerodynamic surfaces and to proceed with the measurement as in the previous case. The latter method is particularly well suited for detection of separated-flow regions. When trying to apply these methods, the experimentalist is presented with some obstacles that are described below:

1. The wire material choice: The search for a suitable wire material was defined in terms of commercial availability in a variety of sizes, price, electrical resistivity, specific heat, temperature coefficient of electrical resistivity, thermal expansion and chemical stability. According to the aforesaid criteria, Chromel emerged as the best practical choice, followed by Constantan.

2. The emittance problem: Since Chromel wires and strips are supplied with polished surfaces, they have very low emittances (approximately 0.05 at room temperature). This fact raises two problems; first, because of the low emittance (and hence, high reflectance), one may get false signals from reflections of heat sources in the vicinity of the target. The likelihood of this phenomenon increases with the dimensions of the target (wire or strip). The second problem arises when the heated element is bonded to a substrate with a much higher emittance (e.g., wood). In this case, even though the substrate is at a temperature equal to or lower than the heated element, it will appear on the IR display as a much "brighter" and hence hotter object. This fact may cause severe problems in data reduction as the IR image is processed into an actual temperature field.

3. In the same context of a heated element bonded to a substrate, it is important to remember that the substrate is actively involved in the heat transfer process both in the conduction mode with the heated element and in the convection mode with the flowfield, thus inducing a phase lag in the target's time response. This complex coupled heat-transfer analysis in conjunction with measurements involving hot-film sensors is treated in [4].

4. The resolution problem: In terms of measurement accuracy, the best approach is to work with a target (heated wire) as thin as possible. This arrangement gives a faster time response and minimizes the heat conduction along the wire, background reflection, flow contamination and boundary-layer tripping. However, such a choice is highly detrimental from the IR imaging system's point-of-view. The problem arises when the angle through which the target is viewed by the camera falls below its angular resolution. This means that the camera's IR detector will get less photons from the target than it would get from a target wide enough to fill a whole pixel. Practically, this translates into reported temperatures lower than the actual ones. The low emittance of the wires only aggravates the problem. A possible solution to this problem is to assign emittances lower than the actual ones in order to compensate the detector for its lack of saturated target area. This corrected emittance can be determined by calibration versus a known target temperature. It must be realized that since the result of the calibration is influenced by:

a. target distance
b. target size
c. target true emittance
d. the lens' field of view,

a specific calibration is good only for the particular conditions under which it was performed. Therefore, each test configuration requires its own calibration.

5. The out-of-focus background: When scanning targets at very close distances, the background may be out-of-focus, causing its emitted photons to be "smeared" out, contributing an erroneous signal at the detector. This may cause

abnormally (false) low temperatures to be attributed to the background. While a solution was not found for this situation, one should be aware of its existence.

6. The flow regime influence on heat transfer coefficients: When making measurements of convective heat transfer phenomena, one has to remember that the flow may be laminar or turbulent, thus exhibiting different heat transfer coefficients in the same field of view. Therefore, differences in temperatures should be analyzed carefully in order to trace them back to their origin; namely, either changes in velocity or changes in flow regime or both.

The aforesaid points illustrate the range of problems that were encountered during this experimental research. Simple flowfield experiments were initially chosen in order to ease the task of resolving the IR imaging and data reduction problems.

4. EXPERIMENTAL RESULTS

Several different experiments were performed in order to demonstrate the various possible applications of the IR imaging system. In what follows, the experiments and their objectives will be presented to illustrate the experimental method.

1. Air-jet heated suspended wire:

The purpose of this experiment was to check the dynamic capability of the AGA system by monitoring a temperature transient. The general experimental layout is shown in Figure 1. A 0.003" Chromel-Constantan uninsulated thermocouple wire was placed 0.33-m above the nozzle of a heat-gun. At time t=o, the power switch was turned from the "heat" position to the "cool" position, while the air continued to flow cooling the heating element of the heat-gun. The airflow was aimed at the region of the thermocouple junction, thus enabling a comparison of the data obtained through the AGA system with the thermocouple output. Sixteen consecutive frames of the suspended wire were taken at 0.7 sec. intervals. In parallel, the thermocouple output was recorded on a strip chart-recorder. The results are displayed in Figure 2, where one can see qualitative agreement between the results obtained with the two independent instruments. The discrepancy at t=o is due to the relatively slow initial time response of the chart-recorder. Ten more identical experiments were carried out at different times with similar results, thus proving their repeatability. However, when the same experiment was run with much larger diameter wires (0.015"), the results obtained were not satisfactory, with the AGA system consistently showing, during early times, higher temperatures than the thermocouple readings. This was explained by the possible interference of the heat-gun IR radiation which reflected from the wire to the camera.

2. Electrically heated suspended wire locally cooled by an airstream:

The purpose of this experiment was to check the resolution capability of the AGA system in monitoring temperature gradients along the wire. The test system for this experiment was identical to that shown in Figure 1, except for the fact that the 0.003" thermocouple wire was heated by an electric current, and the local cooling was achieved with a low-speed airjet (1.5 cm in diameter), flowing perpendicularly to the wire. The effective air velocity at the wire was checked with a Pitot probe and found to be $\approx$ 2.5 m/sec, which gives at 22C a Reynolds number based on the wire diameter of $Re_D \approx 11.5$. In this regime the flow is laminar and the Nusselt number from a standard correlation [5] is about 2.0, giving a heat transfer coefficient of h = 725 W/m^2K. Alternatively, from the IR image as shown in Figure 3, the area of maximum effective cooling is about 1 cm long, and the wire temperature ($\sim$ 42C) is about 20C above the jet temperature. With an applied voltage of 22V and a total wire resistivity of 152 Ω, the current through the wire was 0.144 A, which resulted in a heat dissipation rate of 0.034 W at the location of maximum cooling. The subsequent local heat transfer coefficient of 726 W/m^2K is in fortuitous agreement with the result determined from the correlation.

This experiment and the crude calculation comparing its result with a standard correlation for forced convective heat transfer suggests that through Stanton number correlations, flowfield velocity variations can be traced back to local temperature measurements.

3. Measurements in the wake of a cylinder:

Measurements were made in the wake of a 0.1-m diameter cylinder. These tests were conducted in a 3'x4' low-speed wind tunnel. The 0.003" wire was placed perpendicularly to the flow direction and to the axis of the cylinder at 0.3-m from the wind tunnel floor and parallel to it. The cylinder was placed five diameters upstream of the wire and the IR camera was located 0.5-m downstream of the wire, looking upstream at both the wire and the cylinder as shown in Figure 4. At a freestream velocity of 14.3 m/sec, the Reynolds number $Re_D \approx 90000$. The thermocouple wire could be used alternately as a thermocouple and as an electrically heated sensor wire. The wire's thermal dissipation maintained its temperature at about 50C above the freestream value. Figure 5 shows the result of the experiment. Although the mean air velocity in the wake is lower than in the freestream, the heat transfer coefficient is higher due to the turbulent vortical flow. In particular, it is interesting to observe the effect of the main vortices at the wake's edges where the heat transfer rate is visibly higher than at its core. In a related experiment, a 2-cm diameter cylinder

was placed 24 diameters upstream of the heated wire at an air velocity of 14 m/sec. The temperature distribution along the wire is presented in Figure 6. Such experiments were carried out with wires placed between 8 to 32 diameters downstream of the cylinder. The wake's signature on the wire was very visible on the IR display, proving the system's capability of capturing the effect of wakes even with wires at relatively large distances behind the source of the disturbance.

4. Flat plate measurements:

The last two experiments to be reported herein were aimed at reproducing two classical experiments in aerodynamics: the laminar velocity and thermal boundary layer development along a flat plate at zero angle-of-attack and flow over a rearward-facing step. For this purpose, a vertical flat plate with a 1.0-m span, 0.3-m chord and a sharp leading edge was placed vertically in the wind tunnel previously described. A 0.003" Constantan wire was wrapped three times around the plate chordwise and at 1-cm pitch. A 2" wide aluminum tape was applied over the wires, from the leading to the trailing edge to ensure uniform surface texture and heating. The wires were heated by a constant electrical current. The IR camera was placed laterally 0.5-m from the target plate, behind another plate (parallel to the first one) with a circular hole in it through which the camera could view the target. This was done in order to prevent vortices shedded from the camera from interfering with the flow over the target plate. The result for a velocity of 14 m/sec. is presented in Figure 7. The Reynolds number at a distance x=16-cm from the leading edge is 131000, so that the boundary layer is laminar all along the plate [6]. The temperature irregularity at the leading edge of the plate was due to IR background reflections from the aluminum tape. The result obtained is self evident. For comparison purposes, one may use Reynolds' analogy (i.e., Prandtl number of unity) and therefore assume similarity between the velocity and thermal boundary layer growth. Such a comparison with the data available in the literature [7] shows that the measured profile is qualitatively correct, indicating the true potential of the IR imaging system, i.e., simultaneous temperature mapping along a line, and ultimately over a surface, with minimal effort on the part of the investigator.

Finally, qualitative data relating to flow over a rearward-facing step will be reported. On the same flat plate described earlier, a 30-degree wedge terminating with a 5-cm long and 2-cm high step was fixed to the plate, thus creating a rearward-facing step geometry for the flow. The step was placed over the heated strip reported earlier, and was covered with aluminum tape in order to maintain a uniform emittance in the target area. The results for an air velocity of 14 m/sec. are shown in Figure 8. One can clearly observe the increase in the flat plate's temperature due to the low velocities just behind the step. As the flow approaches the reattachment point, the temperature goes down once again until the minimum is achieved in the vicinity of the reattachment point, in agreement with the expected behavior. Further downstream, the temperature goes up as the boundary layer starts redeveloping. An interesting point to note is that the flow reattachment occurs about 12-cm downstream of the step (about 6 height steps), which is in good agreement with results reported in the literature [8].

5. SUMMARY

The infrared imaging system, when properly and carefully used, has proven to be a viable experimental tool applicable to aerodynamic research. The scanning of actively-heated aerodynamic surfaces can produce very useful data on forced heat transfer, velocity distribution, boundary-layer flows, separated flows and wakes. The method also has a limited capability for capturing transients. This limitation is not conceptual but is due primarily to the low scanning and data aquisition rates characteristic of the available hardware.

Typical results have been reported here for a series of simple aerodynamic experiments. Confidence has been gained in the use of IR surface imaging as a flow diagnostic device, especially since the relatively crude initial experiments display good data repeatability for both steady-state and transient temperature fields. Work is continuing in order to develop the technique as a low-speed quantitative tool with obvious extensions to high-speed aerodynamics.

ACKNOWLEDGEMENT

The authors wish to acknowledge Mr. E. W. Cronce and Mr. K. Ferguson from the College of Engineering and Technology at Old Dominion University for their dedicated technical support of this research.

This research was supported in part by NASA grant NAG-1735.

REFERENCES

1. Meroney, R. N., Studying the Convective Heat Transfer from a Building Model with Infrared Camera Techniques, ASME Paper No. 78-WA/HI-58.

2. Schmitt, R. L. and Chanetz, B. P., Experimental Investigation of Three Dimensional Separation on an Ellipsoid-Cylinder Body at Incidence, AIAA-85-1686.

3. Bouchardy, A. M. Durand, G. and Gauffre, G., Processing of Infrared Thermal Images for Aerodynamic Research, Applications of Digital Image Processing, April 19-22, 1983, Geneva, Switzerland, pp. 304-309.

4. McRee, G. J. and Judge, D., Proceedings of the 12th International Congress on Instrumentation in Aerospace Simulation Facilities, College of William and Mary, Williamsburg, Virginia, June 22-25, 1987 (present Congress).

5. Wong, H. Y., Handbook of Essential Formulae and Data on Heat Transfer for Engineers, Longmans, 1977, p. 76.

6. Schlichting, H., Boundary Layer Theory, McGraw-Hill, 6th ed., 1968, p. 39.

7. Schlichting, H., Op. Cit., p. 132.

8. Selby, G. V., Phenomenological Study of Subsonic Turbulent Flow over a Swept Rearward-Facing Step, Ph.D. Dissertation, University of Delaware, June 1982.

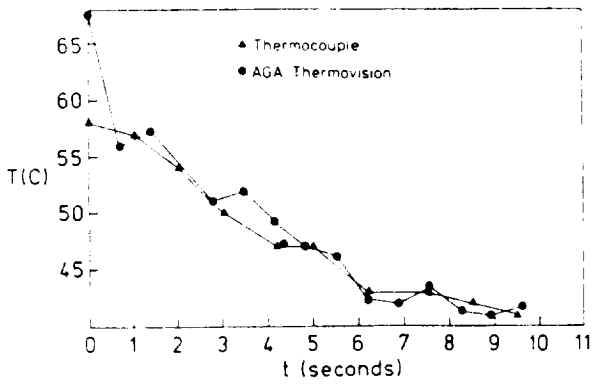

Fig 2 Heat-gun airstream cool-down process as monitored through a 0.003" thermocouple wire suspended at 33 cm above the nozzle

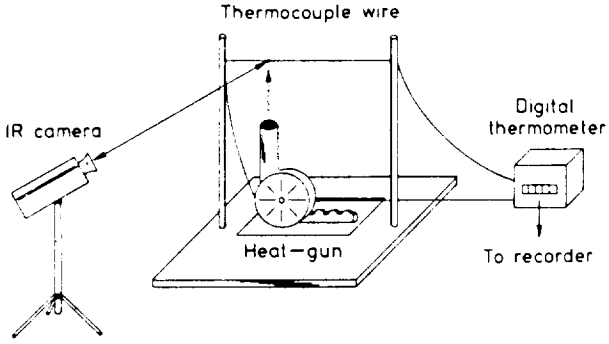

Fig. 1 Experimental set-up for the air-jet heated suspended wire.

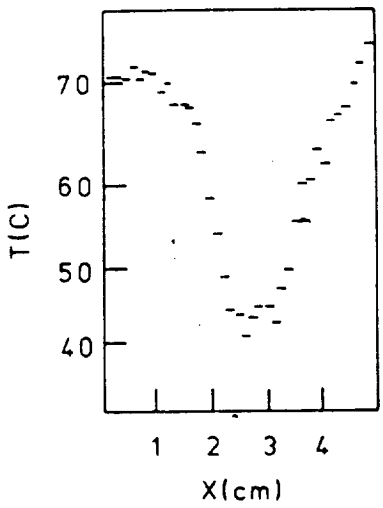

Fig. 3: Temperature variation along a 0.003" electrically heated wire placed in a 2.5 m/sec. airjet at 24C.

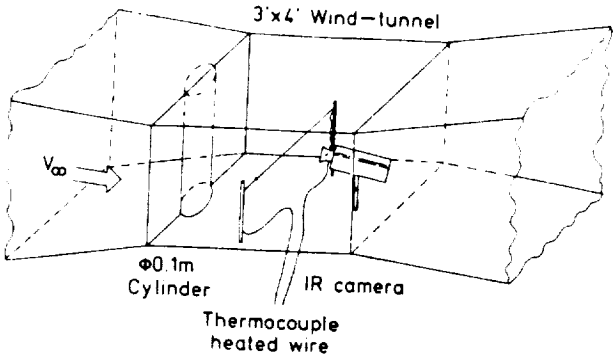

Fig. 4: Experimental layout for IR measurements of a heated wire in the wake of a cylinder

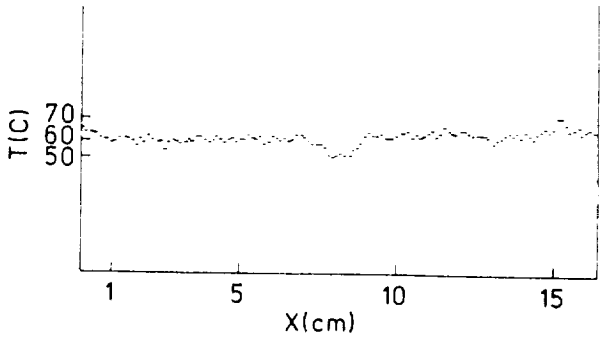

Fig. 6: The wake of a 2 cm diameter cylinder as captured on a 0.003" electrically heated wire placed 24 cylinder diameters downstream. $Re_D = 18,000$.

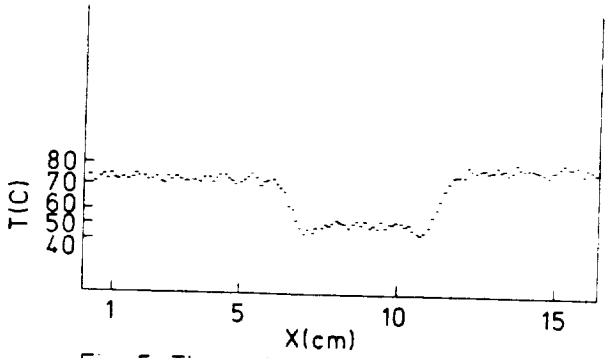

Fig. 5: The wake of a 10 cm diameter cylinder as captured on a 0.003" electrically heated wire placed 5 cylinder diameters downstream. $Re_D = 90,000$.

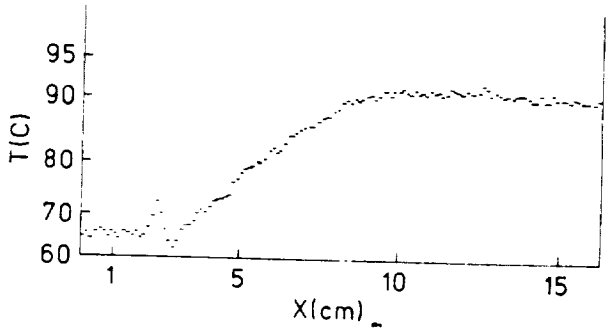

Fig. 7: Temperature distribution along a heated flat plate. $V_{air} = 14$m/sec.

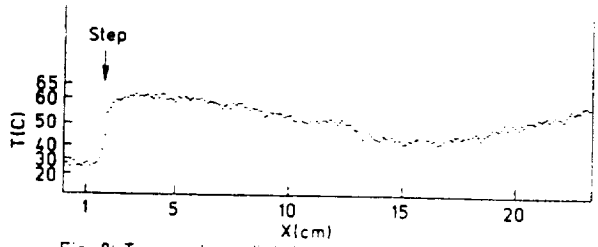

Fig. 8: Temperature distribution over a heated plate with a rear facing step. $V_{air} = 16$m/sec. Step height = 2 cm

Ehud Gartenberg, B.S. and M.S. in Aeronautical Engineering from the Technion, Haifa, Israel; currently a Ph.D. student at the Department of Mechanical Engineering and Mechanics, Old Dominion University. His professional experience is mainly in testing aeronautical and propulsion systems.

A. Sidney Roberts, Jr., with B.S. and Ph.D. degrees in Nuclear Engineering from N.C. State University and the M.S. in Mechanical Engineering from the University of Pittsburgh, PA, USA, has general interests in power/energy conversion systems and particular interests in experimental fluid mechanics and heat transfer. At Old Dominion University, where he is Professor of Mechanical Engineering and Mechanics, research has been accomplished recently in the areas of the melting problem, creeping flows, energy and mass transfers in buildings, and the development of infrared imaging for flow field detection.

Gregory V. Selby has a B.S. degree in Aerospace Engineering from the University of Virginia and M.S. and Ph.D. degrees from the Mechanical and Aerospace Engineering Department of the University of Delaware. His professional experience includes 12 years with NASA performing engineering analyses on sounding rocket systems and conducting research in fluid mechanics. He is currently an assistant professor at Old Dominion University with research interest primarily in the areas of flow visualization, low-speed drag reduction and control of separated flows.

AIAA'88

AIAA-88-2523-CP
Aerodynamic Investigation by Infrared Imaging

Ehud Gartenberg, A. Sidney Roberts Jr. and Griffith J. McRee, Old Dominion Univ., Norfolk, VA

AIAA 6th Applied Aerodynamics Conference

June 6-8, 1988/Williamsburg, Virginia

AERODYNAMIC INVESTIGATION BY INFRARED IMAGING

88-2523-CP

Ehud Gartenberg*, A. Sidney Roberts, Jr.**
and Griffith J. McRee***

Old Dominion University
Norfolk, Virginia 23529-0247

Abstract

Infrared imaging systems can be used to measure temperatures of actively heated bodies immersed in an airstream. This monitoring of the convective heat transfer process, provides also information about the interaction between the body and the flow. The concept appeals to Nusselt/ Reynolds numbers relations in order to produce data of interest from surface temperatures. Two test cases are presented and reference is made to analytical results: the mapping of a laminar jet and the temperature distribution along a constant power heated flat plate in laminar boundary layer regime. Although this research is currently focused on low speed aerodynamics, the extension to high speed aerodynamics, where the body undergoes frictional heating is of interest in this context, too.

Nomenclature

k	thermal conductivity
$\dot{q}_o''$	heat flux (per unit time per unit area)
T	absolute temperature
U	freestream velocity
X	coordinate value in stream-wise direction
θ	differential temperature ($= T_{wall} - T_\infty$)
ν	kinematic viscosity
Nu	Nusselt number
Pr	Prandtl number
Re	Reynolds number

1. Introduction

The traditional experimental tool in aerodynamics is the Pitot tube. Using the exchange principle between the kinetic energy of the flow and its pressure, this device measures pressures from which corresponding velocities can be determined. These measurements are by their very nature, pointwise valid and intrusive. For mapping a region of interest, the choices are either to move the probe from point to point within the flowfield, thus introducing uncertainties associated with time-dependent phenomena, or to introduce into the flow a pressure rake consisting of an array of individual probes, thus perturbing the flow exactly at the points of interest.

An alternative approach may use the principle of thermal exchange between the configuration of interest and the surrounding flow. Starting from this principle, one may assume that by measuring the temperature distribution over an aerodynamic surface, the local freestream velocity may be deduced through a Nusselt-Reynolds type relation approach. This concept is diagrammatically shown in Figure 1. With the renewed interest in high Mach number flows, where the aerodynamic and the thermal loads (with the resulting structural response) are coupled, the infrared imaging technique arises as a natural experimental choice. The advantages it offers are that it's non-intrusive, area-scanning, readily available and has plenty of supporting software and hardware that is developed not necessarily for aerospace applications, thus reducing instrument development costs.

In this research use was made of actively heated bodies and very low speed airflows in attempting to isolate every factor that may influence the measurements and assess quantitatively its influence on the final results. The main factors include:

1) The flow velocity
2) The heat exchange rate and surface overheat
3) The target material and its surface properties
4) The lens field of view
5) The camera distance to the target
6) The ambient temperature

With increasing airflow velocities and the respective Mach numbers, the concept of active heating should be discarded in favor of passive heating due to the increasingly higher recovery temperatures at the wall. The latter concept is valid as long as the gas in the immediate vicinity of the configuration stays radiatively non-participating. In the high Mach-number flow regimes (super-and-hypersonic) when the surrounding gas starts to be radiatively participating (and eventually chemically unstable), this technique maintains its vitality provided the sources of radiation are properly associated with their respective measured temperatures. However, in this paper results are reported for actively heated surfaces and low speed flows.

The target surfaces may be of two distinctive types:

* Ph.D. student, Aeronautical Engineer, Member AIAA
** Professor of Mechanical Engineering
*** Associate Dean, College of Engineering and Technology

1) They may be the aerodynamic configurations themselves, the data obtained being influenced also by boundary layer behavior, i.e., laminar, turbulent, transitional or separated.

2) They may be very thin (heated) wires, interfering to a minimum with the surrounding flow and thus particularly well suited to detect or map wakes, jets, shear-flows or any other non-uniform flows.

In the early phase of this investigation a series of experiments were designed and carried out in order to check qualitatively how this concept works. Widely different types of flow such as laminar jets, wakes, laminar boundary layer growth and separated flows over a rear-facing step were mapped with very promising qualitative results[1].

2. The IR Imaging and Processing System

The nucleus of the IR imaging system is an AGA Thermovision 782 camera equipped with 20°x20° lens coated for optimal response in the short wave (5 μm) infrared spectrum. At 0.5-m distance, the field of view is 0.15 x 0.15-m. Throughout the reported experiments, the aperture was kept at f/1.8. The optical scanning system is syncronized such that four fields of 100 horizontal lines each, produce one interlaced frame. The scanning rate is 25 fields per second. The scanned field is reproduced on a specially-designed black-and-white video display unit, which facilitates direct or relative thermal level measurements. The angular resolution of the system in the above configuration is 0.003 radians.

The digital image processing is performed on a dedicated BMC IF800, model 20 personal computer with 64K bytes main memory plus an extra 128K bytes RAM PCB and two 5 1/4" disk drives. The color CRT display has graphics capability.

A DISCO 2.0 software package is used for the image processing and completely occupies a floppy disk in a read-only storage mode. Up to 36 individual images, which can be either fields or frames, can be stored on the second floppy disk in a read-and-write access storage mode. The automatic aquisition capability of the system permits continuous recording of up to 16 images at an approximate rate of 1.5 Hz or lower. Although both the field and frame acquisition modes are available, only the field mode was used. A key feature of this program is the gradual assignment of eight tones of artificial colors (from black through blue, green, red, etc., to white), for corresponding grey shades in the original image. Such a display produces a color shade for each temperature band scanned by the camera. The user has the choice of getting temperature measurements at a certain point or along specified rows or columns, for given values of the input parameters (emittance, transmittance, ambient temperature, etc.). Also, the user can concentrate on a given range of temperatures, depending on the area of interest. The program is quite versatile and offers an abundance of processing and filtering choices; however, only the essentials have been reported herein.

3. The Laminar Jet Experiment

The laminar jet experiment was intended to test the capability of mapping flows with position-dependent velocities using the heated wire concept.

In this experiment, the infrared camera mapped the temperature distribution along a thin, electrically heated Chromel wire, part of which was diametrically placed at the exit of a pipe from which a laminar jet discharged into the atmosphere. The measured temperatures were used in conjunction with heat transfer correlations in order to obtain the air velocity distribution within the jet.

The Chromel wire 0.003 inch in diameter (0.0762 mm.) was part of a Chromel-Constantan thermocouple assembly that was previously used for wire emittance calibrations as shown in Figure 2.

Those calibrations were performed as follows: A working heat-gun was aimed at the thermocouple's junction, thus getting a direct reading of the wire's temperature. This temperature was double-checked with a mercury thermometer. In parallel, the wire was thermographed by the AGA system and the temperature of the Chromel wire adjacent to the thermocouple's junction was analysed with the Disco 2.0 software on the system's microcomputer. The emittance input of the wire was adjusted until the result from the computation equaled that of the thermocouple readout. This result was checked with another software package supplied by AGA and run on an HP-41 CV programmable calculator with identical results. The Chromel wire length was 40 cm. and the Constantan wire length was 10 cm. The thermocouple assembly was hung between two vertical bars 50 cm apart. The length to diameter ratio of the Chromel wire was 5250:1, so that the influence of the heat conduction (in the area of interest) to the supports can be neglected. The wire was heated by a D.C. electric current passing through it. The laminar flow pipe exit was placed at 1 mm. distance from the heated wire, at the center of the Chromel section, as shown in Figure 3. The air-supply pipe had a 0.545 inch (13.353 mm) internal diameter and a straight section of 80 cm., thus getting a length to diameter ratio of 60. The air was supplied by a standard 100 psi low-pressure supply system (of the type that is usually found in laboratories and workshops). The air mass-flow rate was determined by taking total pressure and temperature measurements upstream of a sonic nozzle. Three fine-mesh screens, (each rotated at 45° with respect to the others) were placed at the entry of the straight section of the tube in order to break down any large vortices or non-uniformities that might exist in the flow. The nominal mean air velocity in the tube was about 2 m/sec, and the corresponding Reynolds number based on the pipe's diameter was about 1700, which is well under the critical Reynolds number of 2300.

The infrared camera was placed at a distance of 0.5 m from the wire. The experiments were carried-out at four different levels of heating corresponding to dissipation rates of 3.97, 9.71, 6.17 and 9.33 watts/m of Chromel wire.

For each separate experiment, 9 consecutive fields were taken at a rate of 1.5 Hz and their average was stored as a single frame on the computer's diskette for latter analysis. During each experiment, the range and level of the camera were carefully set according to the target's luminosity in order to minimize the background noise and at the same time to prevent the detector from being under or overexposed (saturated) to the target's photons. In either case the output result ceases to be proportional to the target's temperature.

The results of the experiments at the three lower heating rates are presented in Figure 4 while the result of the experiment carried out at the highest heating level is presented in Figure 5. The darkened symbols are given for comparison and represent the expected temperature distribution along the section of the wire directly exposed to the laminar flow. The air velocities were calculated assuming parabolic velocity distribution as predicted by the viscous-flow theory. The respective temperatures were deduced from the

$$Nu = 0.795\ Re^{0.384} \qquad 1 < Re < 35 \qquad (1)$$

cross-flow correlation[2]. In this case the Reynolds number at the computed points varied roughly between 4 to 20. The most striking feature of these results, is the ever increasing discrepancy between the measured versus the expected temperatures predicted by correlation (1), for decreasing Reynolds numbers. Since this correlation accounts only for forced convective heat transfer, a first thought was to check the possible contribution of the other two heat transfer modes, namely conduction and radiation. The radiation effect can be discarded from the onset. Assuming that the emittance and the absorptance of the wire's material are the same, one gets for an overheat of 80° K above the room ambient that the radiation effect is three order of magnitudes lower than the generated heat. For evaluating the possible heat conduction contribution, the temperature profile of the wire exposed to the highest overheat was approximated by a cosine-type function fit between 0 and π radians. With a maximum temperature gradient of 2524 °K/m and a mean conductivity coefficient of 50 W/m°K, the maximum conductivity loss for a wire element between two adjacent sampling points is still two order of magnitudes lower than the generated heat; therefore, this mechanism can be discarded too. One possible conclusion may be that the forced convective heat transfer correlations reported in the literature may not be applicable all along the specified range of Reynolds numbers, even though the conditions themselves seem at least a priori, to fall within the validation limits of the correlation.

In this context, it is of interest to check how well the experimental results are correlated. A quick look at Figures 4 and 5 shows that the scatter of the measured temperatures decreases as the overheat level increases, a fact that may be attributed to a better signal to noise ratio. However, in spite of the apparent advantages of high overheating, it should be remembered that it may cause changes in surface emittance, excessive wire elongation (that may induce high amplitude vibrations) and thermal contamination of the flow. Thus, the overheat value should not be abused.

Further evidence that for lower Reynolds numbers the assumed correlation fails to reproduce the reality is provided by the fall of velocity toward the jet's edge. Starting approximately at Re=5, the predicted temperature is higher than that measured on sections of the wire outside the jet plume were the natural convection was the more significant heat removal mechanism. This result repeated itself on all four experiments, and is of course unacceptable.

The deduction of the velocity profile from the measured temperature profile through Nu-Re correlations is also possible. This time, the process is reversed and using the same correlation, the differential temperature is assumed known when calculating the velocity that would produce it. The results as deduced from the experiment with the highest heating rate are presented in Figure 6. The explanation for the increasing departure of the deduced velocity data (Fig. 6) from the theoretical profile, compared to that of the temperature data from which it was deduced (Fig. 5) lies in the behavior of the Nu-Re correlations. These correlations assume a behavior like $Nu \sim Re^{n}$, $0 < n < 1$. In the former case one gets $\Delta T \sim U^{-n}$, while in the latter $U \sim (\Delta T)^{-1/n}$, thus causing the deduced velocity behavior U to be quite sensitive to the scatter of the temperature measurements. In spite of this fact the results of these experiments show that for Reynolds numbers above 15, good velocity estimations can be obtained even with the existing correlations.

The encouraging aspect of this approach is that as the Reynolds number increases with the velocity, so does the heat transfer coefficient, on a power law basis[2]. The net result of this feature is to increase substantially the accuracy of the velocity predictions from the temperature measurements.

4. The Flat Plate Experiment

The second experiment to be reported herein was aimed at reproducing another classical experiment in aerodynamics: the laminar velocity and thermal boundary layer development along a flat plate at zero angle-of-attack.

The target flat plate measured 32 cm. chordwise, 90 cm. spanwise, was made of wood and had a sharp leading edge of the type assumed in the Blasius analysis of the boundary layer. The IR camera was placed laterally at 55 cm. from the target, behind a second plate (parallel to the first one), with a circular hole through which the camera could view the target. This was done in order to prevent the vortices shedded from the camera from interfering with the flow over the target plate. As shown in Figure 7, the entire

assembly was placed vertically in the department's 3' x 4' low speed wind tunnel where the experiments took place.

The target flat plate was placed in the wind-tunnel at $0^{-0.5}$ degree angle of attack, so that the surface under investigation was at most accelerating minutely the external flow.

The active heating of the target plate was achieved locally, at one third of the span, by wrapping chordwise a 0.00397" Constantan wire three times around the plate at 2 mm. pitch and connecting it to a power supply. To ensure uniform surface texture and roughness, these wires and the entire surrounding area in the field of view of the camera were covered chordwise with three adjacent strips of 2" wide duct tape. At 85 mm. from the leading edge, a Chromel wire was soldered to the Constantan wire and its lead was taken to the back of the plate through a very small hole that was drilled in the wood. This layout enabled emittance calibrations of the duct-tape surface by providing the true surface temperature. Hence, the Constantan wire played a dual role in this experiment, as a heating element when connected to the power supply, or as a thermocouple element when connected to a digital thermometer. The desired function was selected by switching between the circuits. Direct measurements performed during the experiments show that heat was dissipated at a rate of 949 W/m^2 over that area of the flat plate that was affected by the testing.

The guiding rule in performing these experiments was to make them as short as possible. There were two reasons for this, one concerning the wind-tunnel operation, the other concerning the substrate participation in the heat transfer process. Since the wind-tunnel used in this experiment is of closed circuit type, the longer the operation period the higher is its air temperature. This phenomenon has a negative influence on the heat transfer process from the flat plate to the fluid and in general is disruptive to infrared measurements. The other concern was that long periods of heating, would effect the substrate to an unknown degree resulting in long cooling times between runs and irreproducible results. In this respect, the thermocouple used for emittance calibrations proved to be of significant help in establishing the substrate initial conditions for each test.

A total of 20 tests were performed. Of these, eleven tests were recorded. Since the results of all the runs were very much alike, only the last three were picked-up for data analysis. The reproducibility of the results ensured that no further benefit would have come out of analyzing more profiles, except perhaps to establish a statistical variation measure for the data set.

The chordwise temperature profiles as obtained from the last three runs are shown in Figure 8. The camera's field of view in this configuration was 16.5x16.5 cm, and the Reynolds number of that area of the plate scanned by the camera varied between zero (at the leading edge) to about 217000. This means that the phenomena addressed are all under the laminar boundary layer regime.

The data as presented in Figure 8 displays the temperature profile along the plate reduced by the airflow temperature, versus the chordwise coordinate. A primary evaluation of these profiles will reveal the following:

1) The information gathered from all three runs was quite reproducible and the data points obtained from the different experiments almost coincide.
2) The general qualitative behavior of the temperature profile theory meets the expectations based on laminar boundary layer theory.
3) The temperature distribution exhibits some irregularity around the coordinate X=8 cm. This is the region where the thermocouple junction was placed, a fact that caused a slight "bumpiness" on the overlaying duct tape surface. It is assumed that this geometrical feature may have initiated a directional emittance factor, which is usually lower than its normal counterpart. This effect, not being taken into account by the system's softwave, is ultimately (and falsely) interpreted as a local drop in temperature.
4) The leading edge experiences an abrupt increase in its temperature, due to its sharpness. This geometrical feature causes a finite amount of heat to be absorbed by a theoretically infinitesimal substrate mass, with the consequent real increase in temperature. The effect is further augumented by the fact that the heating wires being wrapped around the plate, the leading edge is well heated from all around its contour.

As a result of these considerations, it was decided to proceed with the analysis of the experiments, using only the data points starting at the coordinate X = 1.9 cm from the leading edge (the first 1.52 cm. from the leading edge were ignored). The numerical values of these coordinates resulted from the fact that the data was extracted at each third consecutive pixel, which on the plate is equivalent to an interval of 3.8 mm.

In search for a model against which the experimental results can be evaluated, the physical reality of constant power heating at the wall, suggests using the flat plate laminar boundary layer model with constant heat flux at its surface as the prescribed boundary condition. The model assuming a general heat flux distribution chordwise and its analytical solution was formulated by Tribus and Klein[3]. When simplified to the constant heat flux assumption, the solution reads:

$$\theta(x) = 2.2019 \frac{\dot{q}''_o}{k} Pr^{-1/3} \left(\frac{\nu}{U}\right)^{1/2} x^{1/2}$$

$$= \text{const} \cdot x^{1/2} \qquad (2)$$

According to this model when the flat plate corrected temperature distribution is plotted against the square-root of the distance from the leading edge, the slope of the line is an indication of the heat flux convected into the airstream. When this plotting is done for the present case, as shown in Figure 9, its analysis shows that although the data is well correlated, the assumed linear behavior of the data is not uniform all along the coordinate scale. A closer look suggests one linear regression for the first 14 stations and another for the last 18 stations, leaving 6 stations in between as a transition zone. The question is what causes this change in the pattern behavior. A possible answer lies in the actual physical process taking place with this experimental set-up and its departure from the assumed model. As shown in Figure 10, the theory assumes a flat plate "pumping" a constant amount of heat flux into the airstream. For a desired constant value of this heat flux, a certain prescribed temperature distribution should be maintained (or obtained) in order to compensate for the fact that the boundary layer thickens and heats up streamwise. In this case, the constant heat generation rate is shared mainly by two participating media, the wooden substrate by conduction and the airflow by convection. Heat transfer by radiation is also taking part, but to a lesser degree. Since the air cooling by convection is very effective on the forward part of the plate, (due to the thin boundary layer), the heat transfer by conduction to the substrate is much less than on the aft part of the plate, where the boundary layer is thick and the convective heat transfer is much poorer. The estimation of the boundary layer behavior will show that between the first and the last station of the first data group, it thickens by 90% (from 0.60 mm. to 1.15 mm) while with respect to the second data group, it continues to thicken but only by 30% (from 1.35 mm. to 1.75 mm.). Therefore, the heat conduction mechanism to the substrate will play a more prominent role on the aft part of the plate and contribute to the change of the trend exhibited over its leading part. Looking again at Figure 9, one may further observe that the general trend of the slope of θ vs. $X^{1/2}$ is to decrease gradually from the leading edge downstream, a feature that may add additional evidence to the ever increasing participation of the substrate due to the gradual decreasing effectiveness of the convective cooling.

The thermal energy analysis performed on the flat plates is summarized in Table 1 which clearly shows the gradual shift in the energy transfer mechanism from the predominantly convective mode in the leading edge area to the predominantly conduction mode to the substrate over the downstream regions of the plate. This happens in spite of the fact that the wood qualifies as a heat insulator. The radiative heat transfer mode, although playing a minor role in this configuration, cannot be ignored. Even though the overheat degree was relatively moderate 10 to 20°C, its contribution to the total heat transfer dissipation was about 9%. Theoretically, with different surface conditions and identical overheat values, its contribution could be as small as 1% or as high as 12%.

Table 1: Mean values analysis of the heat transfer modes on a flat plate heated at constant wall power generation placed in an airstream at zero angle of attack. $Re_X = 1.233 \times 10^6 X(m)$.

Data points	X (1)	$\frac{\dot{q}''_{o\ conv}}{\dot{q}''_{o\ gen}}$	$\frac{\dot{q}''_{o\ rad}}{\dot{q}''_{o\ gen}}$ (2)	$\frac{\dot{q}''_{o\ cond}}{\dot{q}''_{o\ gen}}$
All	1.9 → 159.9	42%	9%	49%
1st group	1.9 → 68.5	64%	8%	28%
2nd group	95.2 → 159.9	19%	11%	70%

1. distance from the leading edge (mm)
2. $\dot{q}''_o$ conducted = $\dot{q}''_o$ generated - ($\dot{q}''_o$ convected + $\dot{q}''_o$ radiated), mean value (W/m^2)

conv - convected
gen - generated
rad - radiated
cond - conducted

This experiment shows in a primitive but very fundamental way the potential of using infrared imaging in experimental aerodynamics. Firstly, no other method can supply the temperature distribution so quickly and easily, with no interference with the flowfield, the temperature field, or the geometry of the surface. Secondly, the flat plate temperature profile analysis in a direction perpendicular to the direction of the flow, provided a very easy means to determine very accurately the effective area of heat exchange. The knowledge of this area is critical in establishing the correct value of the heat flux for cases where active heating is employed. Thirdly, the analytical method may be also applied in an identical way to find the freestream velocity U assuming the heat flux is known. This mode will require either a solution to the participation of the substrate in the heat transfer process, or use of a substrate which is highly insulative thermally. Recently, a work which models and simulates highly time dependent coupled convective and conduction heat transfer, was accomplished with regard to hot-film time response investigation[4].

The need to understand the substrate's participation will become more accute in the high-speed regime, where the active heating will give way to frictional heating and the surface temperature distribution might serve as an indication of the aerodynamic loading.

5. Conclusions

The infrared imaging method emerges as a very useful tool in experimental aerodynamics. It can be used to measure temperatures along thin, long, heated wires to map flowfield velocities. A high heating rate of the wire will generally give higher signal to noise ratios, but it can also induce oscillations in the wire due to its thermal elongation. Thus, the optimum operating condition should be a compromise between the two conflicting requirements. Another possibility is to map surface temperatures of aerodynamic configurations to deduce thermal loadings, heat exchange processes and eventually flow velocities. This method gave encouraging results when it was applied to determine the temperature distribution of a constant power heated flat plate in the laminar boundary layer regime. In general, this experimental method focused the attention on the need of better understanding the heat transfer process associated with the coupling between the flowfield forced convection and the substrate participation by conduction.

Acknowledgement

This research was supported by NASA Langley Research Center grant NAG-1-735.

The authors wish to acknowledge Mr. E. W. Cronce and Mr. K. Ferguson from the College of Engineering and Technology at Old Dominion University for their valuable technical support of this research.

References

1. Gartenberg, E., Roberts, A. S., Jr. and G. V. Selby, Infrared Surface Imaging as a Flowfield Diagnostic Tool, Proceeding of the 12th International Congress on Instrumentation in Aerospace Simulation Facilities (Sponsored by IEEE), The College of William and Mary, Williamsburg, Virginia, June 22-25, 1987.

2. Morgan, V. T., The Overall Convective Heat Transfer from Smooth Circular Cylinders, Advances in Heat Transfer, Vol. 11, Academic Press, 1975.

3. Klein, J., and Tribus, M., Forced Convection from Non-Isothermal Surfaces. University of Michigan Engineering Research Institute, August 1952 Project M 992-B.

4. Judge, M. D., Model of Hot-Film Sensor with Substrate Effects, Master of Engineering Thesis, Department of Electrical and Computer Engineering, Old Dominion University, December 1987.

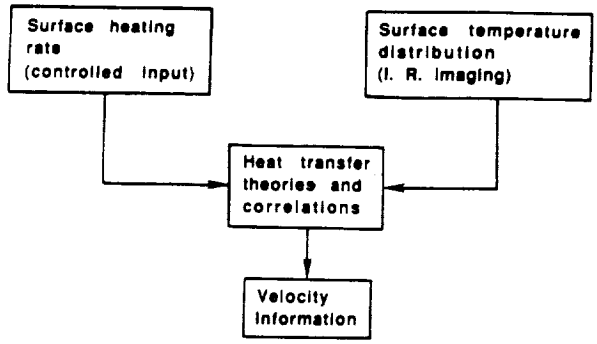

Fig. 1. The concept of flowfield velocity deduction through infrared imaging of the surface

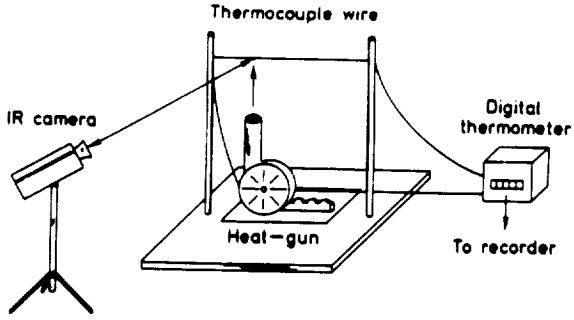

Fig. 2. Experimental set-up for wire emittance calibration

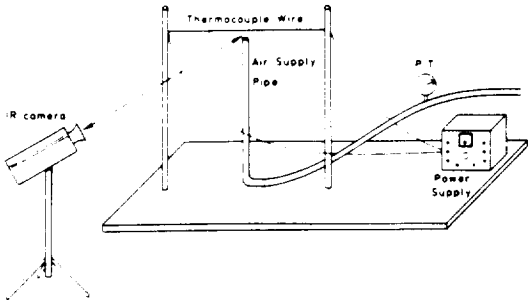

Fig. 3. Set-up for the heated wire laminar jet experiment

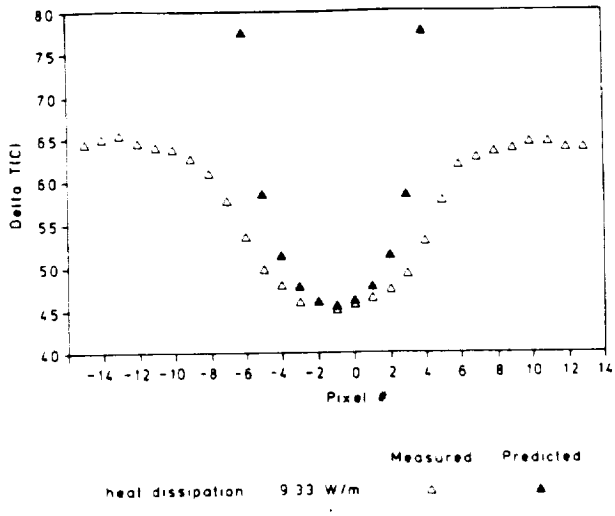

Fig. 5. Heated wire temperature distribution when exposed to a laminar jet. U_{max} = 4 m/sec; 1 pixel = 1.154 mm Prediction based on $Nu = 0.795\ Re^{0.384}$

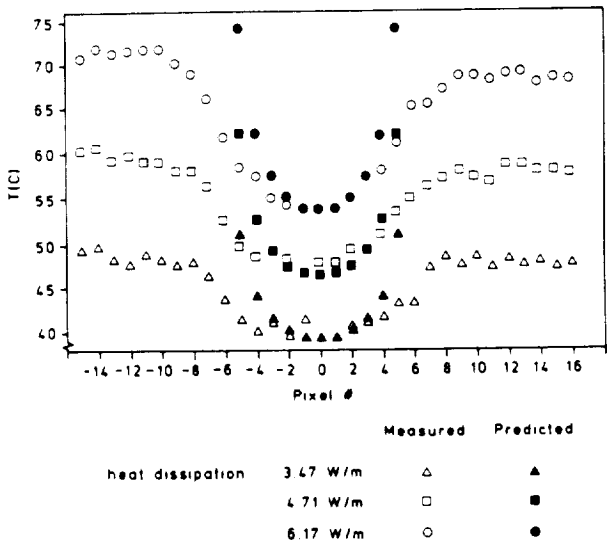

Fig. 4. Heated wire temperature distribution when exposed to a laminar jet. U_{max} = 4 m/sec; 1 pixel = 1.154 mm Prediction based on $Nu = 0.795\ Re^{0.384}$

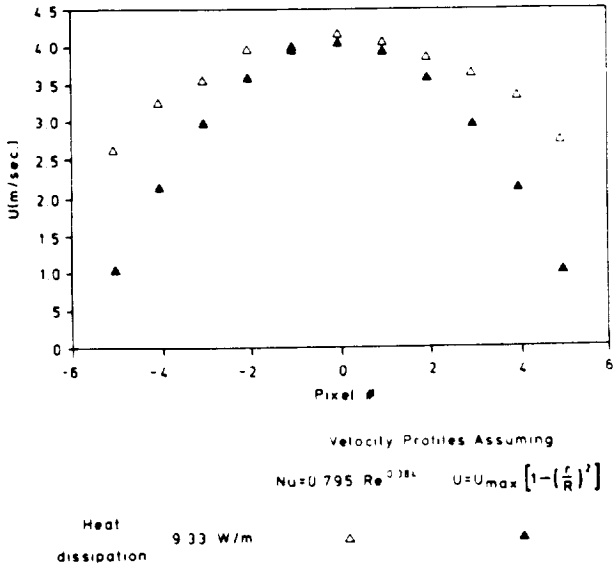

Fig. 6. Velocity profile as deduced from the heated-wire laminar-jet measurements: Nu-Re correlation versus viscous theory solution.

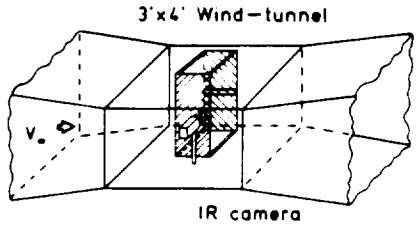

Fig. 7. Layout for infrared imaging surface measurements of a heated flat plate in a uniform freestream.

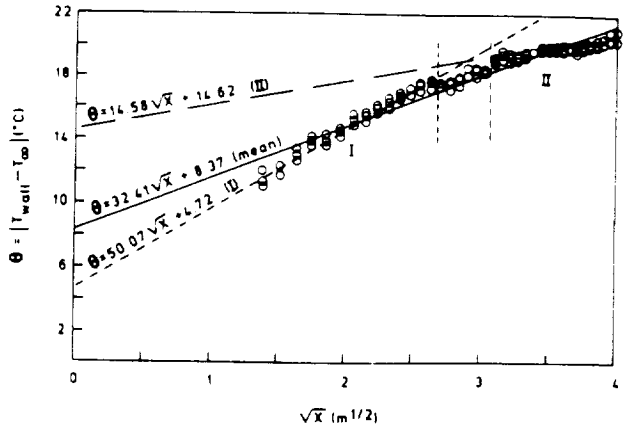

Fig. 9. Constant power heated flat plate experiment: adjusted temperature profile vs. square-root of distance from the leading edge.
$Re_x = 1.233 \times 10^6 X(m)$

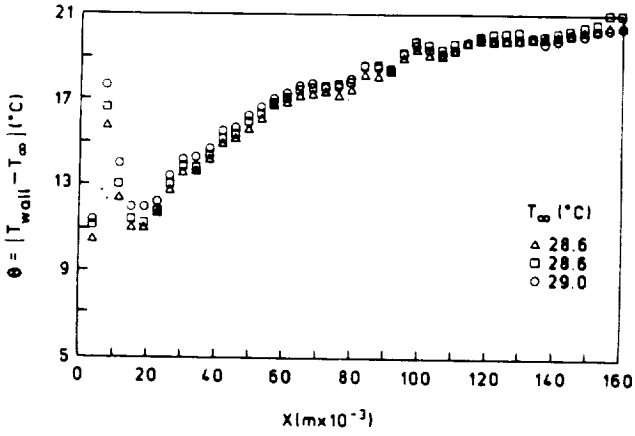

Fig. 8. Constant power heated flat plate experiment: adjusted temperature profile vs. distance from leading edge. $Re_x = 1.233 \times 10^6 X(m)$

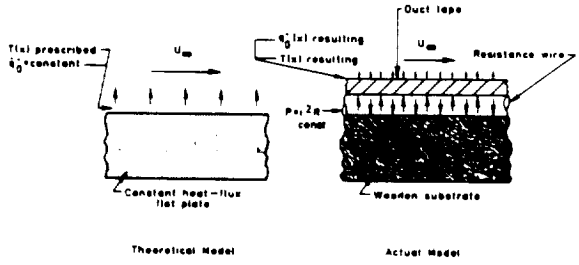

Fig. 10. Heated flat plate experiment: comparison between the theoretical constant heat flux model and constant power reality.